ACS APPLIED MATERIALS & INTERFACES

Research Article

www.acsami.org

Hydrothermal Carbon-Mediated Fenton-Like Reaction Mechanism in the Degradation of Alachlor: Direct Electron Transfer from Hydrothermal Carbon to Fe(III)

Yaxin Qin,[†,‡] Lizhi Zhang,[*,‡] and Taicheng An[*,†]

[†]Guangzhou Key Laboratory of Environmental Catalysis and Pollution Control, School of Environmental Science and Engineering, Institute of Environmental Health and Pollution Control, Guangdong University of Technology, Guangzhou 510006, China

[‡]Key Laboratory of Pesticide & Chemical Biology of Ministry of Education, Institute of Environmental Chemistry, College of Chemistry, Central China Normal University, Wuhan 430079, P. R. China

Supporting Information

ABSTRACT: As Fenton systems suffer from the undesirable Fe(III)/Fe(II) cycle, great efforts were made to realize the effective reduction of Fe(III) to Fe(II). The effects of hydrothermal carbon (HTC) on the Fe(III)/H_2O_2 Fenton-like reaction and the subsequent degradation of alachlor in water was systematically investigated, and the results indicated that HTC could enhance alachlor degradation in Fe(III)/H_2O_2 by promoting the Fe(III)/Fe(II) cycle via electron transfer from HTC to Fe(III) ions. The apparent alachlor degradation rate constant in the HTC-G/Fe(III)/H_2O_2 system (7.02×10^{-2} min^{-1}) was about 3 times higher than that in the Fe(III)/H_2O_2 system (2.25×10^{-2} min^{-1}). The electron spin resonance spectra analysis revealed that HTC consists of abundant carbon-centered persistent free radicals to act as the electron donor. Meanwhile, the hydroxyl groups on the surface of HTC also played an important role in the enhanced alachlor degradation because the decrease in the surface hydroxyl groups on HTC significantly decreased the degradation of alachlor. On the basis of these results, an Fe(III) complex with surface hydroxyl groups on HTC was proposed to favor the electron transfer from the hydroxyl groups to Fe(III), and then, the simultaneously produced Fe(II) could accelerate the catalytic decomposition of H_2O_2 to facilitate alachlor degradation. These findings shed new light on the possible roles of carbon materials in a natural aquatic environment and provide a new pathway for environmental pollutant control and remediation of organic contaminants by HTC.

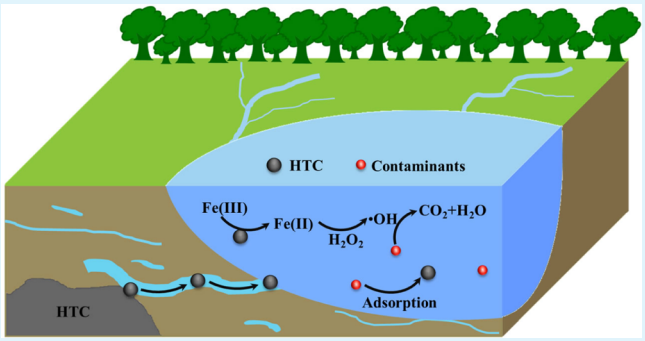

KEYWORDS: *hydrothermal carbon, fenton-like reaction, Fe(III)/Fe(II) cycle, electron transfer mechanism, alachlor degradation*

1. INTRODUCTION

In recent decades, water pollution has become a global issue, especially the persistent organic pollutants (POPs) in various aquatic environments, which have caused a serious threat to human health.[1−3] In view of the recalcitrance and toxicity, POPs cannot be degraded using traditional chemical and biological technologies. Many researchers paid much attention to the degradation of POPs and found that advanced oxidation processes (AOPs),[4−6] such as photocatalytic oxidation and ultrasonic treatment, show great potential in the degradation of POPs through the formation of highly reactive and nonselective hydroxyl radical (•OH).[7,8] Among AOPs, Fenton systems have been extensively studied because of their high efficiency, simplicity, and environmental friendliness to some extent. However, Fe(II) ions are rapidly exhausted by H_2O_2, and Fe(III) ions are quickly accumulated in the Fenton system because the reaction rate of Fe(II) ions with H_2O_2 is much faster than that of Fe(III) ions with H_2O_2.[9] Moreover, Fe(III) ions are inclined to precipitate as iron hydroxides and thus block the Fe(III)/Fe(II) cycle and slow down Fenton reactions.[10] Hence, it is very meaningful to accelerate the Fe(III)/Fe(II) cycle in the Fenton systems.

Carbon materials with controllable sizes and shapes have gained considerable attention owing to their applications in environmental remediation because of their ubiquitous existence in natural environments.[11−14] Many researches have reported that hydrothermal carbon (HTC), a kind of carbon material, can effectively absorb hazardous organic compounds such as bisphenol A, diclofenac sodium, salicylic acid, flurbiprofen, phenanthrene, and so on.[15,16] For instance, Fernandez et al. investigated the adsorption ability of HTC and found that the morphology and surface functionalities of HTC and the solution pH significantly influence the removal efficiencies of three pharmaceuticals, diclofenac sodium,

Received: March 7, 2017
Accepted: May 3, 2017
Published: May 3, 2017

DOI: 10.1021/acsami.7b03310
ACS Appl. Mater. Interfaces 2017, 9, 17115−17124

salicylic acid, and flurbiprofen.[15] Recent studies have indicated that carbon materials can also act as catalysts for the degradation of organic contaminants.[17−22] For example, Gomes and co-workers compared the H_2O_2 catalytic decomposition activity of commercially activated carbon, carbon xerogel, multiwall carbon nanotubes (MWCNT), graphene oxide (GO), and graphite using glycerol-based carbon material and found that commercially activated carbon would be able to catalyze H_2O_2 decomposition.[18] Wang et al. investigated the ozonation of *p*-hydroxylbenzoic acid catalyzed by commercial MWCNT, GO, and reduced graphene oxide (rGO) and found that rGO exhibited much higher catalytic ozonation activities than commercial MWCNT and GO in the degradation and mineralization of *p*-hydroxylbenzoic acid.[19] Zhou and co-workers also revealed that biochar synthesized by the pyrolysis of biomass could activate O_2, H_2O_2, and persulfate through a direct single-electron transfer process to produce reactive free radicals for the subsequent degradation of organic contaminants.[20−22] They suggested that the abundant phenol or quinone moieties in biochar generated during the pyrolysis of biomass could transfer the electron to the transition metals in biochar and then form surface-bound persistent free radicals (PFRs) in biochar. These PFRs in biochar could also act as an electron donor to other activated species. In addition, the carbon materials can also function as an electron shuttle in some cases. Kappler et al. reported that biochar could facilitate the electron transfer from Fe(III)-reducing bacteria to Fe(III) minerals[23] because per gram of biochar can accept or donate several hundred micromoles of electrons because of its abundant phenolic and quinone moieties.[24] However, most of the present research is focused on the adsorption ability of HTC; other environmental applications of HTC such as catalysis and the reduction ability have not been extensively studied.

HTC is generally produced with the hydrothermal carbonization process designed to simulate natural coalification, which usually occurs in an energy-saving manner at a relatively low temperature (180−260 °C) and a self-generated pressure (2−6 MPa) in pure water.[25−27] It is thus attractive for its lower reaction temperatures than those used for pyrolysis and in environmentally friendly solvents (such as water).[28−30] Various kinds of renewable biomass, including saccharides (e.g., glucose, fructose, and starch), lignocellulosic materials (such as wood, grass, and agricultural residuals), and nonlignocellulosic materials (such as animal and municipal solid wastes), could be used as the precursors of HTC, and the biomass could be used without predrying requirement.[31,32] Moreover, the hydrothermal carbonization process does not generate large amounts of harmful gases, and most of the starting carbon remains in the final product, resulting in a high yield of HTC.[33−35] Therefore, HTC was synthesized through environmentally friendly one-step hydrothermal carbonization of saccharides under relatively mild conditions (180 °C and self-generated pressure in pure water). It has been reported that HTC exhibited a type of core−shell structure composing of a hydrophobic core (containing stable oxygen-containing groups such as ether, pyrone, or quinone) and a hydrophilic shell (containing a large number of reactive oxygen-containing functional groups such as hydroxyl/phenolic, carbonyl, or carboxylic).[35,36] Therefore, HTC is more hydrophilic than biochar because of the presence of abundant reactive oxygen-containing functional groups; hence, the adsorption capacity of HTC has been proved to be considerably higher than that of biochar in some cases.[37,38] In view of the hydrophilic nature and excellent adsorption ability of HTC, it is a promising candidate for the remediation of water pollution. As it is well-known, HTC widely exists with ferric ions and hydrogen peroxide in aquatic environments,[39,40] and their interaction might influence the migration and transformation of organic contaminants by affecting the Fenton-like reaction in the natural environment. Unfortunately, no relevant study has been reported on this topic.

In this study, alachlor was chosen as the model organic contaminant to evaluate the influence of HTC on the Fe(III)/H_2O_2 Fenton-like system. Electron spin resonance (ESR) and attenuated total reflectance−Fourier transform infrared spectroscopy (ATR−FTIR) analyses were used to confirm the types of PFRs and surface functional groups on HTC. Simultaneously, the forms and concentrations of iron ions were also monitored to clarify the effect of HTC on the Fe(III)/H_2O_2 Fenton-like system. Then, the effects of precursors and the surface oxygen-containing functional groups on the reactivity of HTC were also carefully investigated. The influence mechanism of HTC on the alachlor degradation efficiency in the Fe(III)/H_2O_2 Fenton-like system was also discussed in detail. The purpose of this study aims to provide more detailed information of the influence of HTC on the migration and transformation of organic contaminants in the natural environment through the Fenton-like system.

2. EXPERIMENTAL SECTION

2.1. Chemicals and Materials. D-Glucose, sucrose, fructose, starch, $Fe(NO_3)_3{\cdot}9H_2O$, hydrogen peroxide (H_2O_2, 30% in water), acetic acid, hydroxylamine hydrochloride, sodium acetate (NaAc), isopropanol, methanol, ethanol, 1,10-phenanthroline, $NaBH_4$, and NaOH were all of analytical grade and purchased from Sinopharm Chemical Reagent Co. Ltd., China. Alachlor was purchased from Sigma-Aldrich. Acetonitrile, acetone, and dichloromethane of high-performance liquid chromatography (HPLC) grade were obtained from Merck KGaA. All chemicals were used as received without further purification. Deionized water was used in all experiments, and H_2O_2 stock solution was prepared by diluting 30% H_2O_2. Fe(III) stock solution with a concentration of 0.04 mol/L was prepared by directly dissolving $Fe(NO_3)_3{\cdot}9H_2O$ in deionized water (pH = 3.7). The concentration of alachlor stock solution was 20 mg/L (pH = 6.8). All other stock solutions were prepared immediately before use.

2.2. Preparation of HTC. In a typical synthesis procedure, 6 g of D-glucose was dissolved in 60 mL of deionized water in an 80 mL Teflon-lined autoclave. The mixture was stirred for 0.5 h at room temperature and then heated at 180 °C for 10 h. The precipitates were collected by centrifugation and washed with deionized water and ethanol thoroughly. Finally, the precipitates were dried in vacuum at 60 °C for 24 h and labeled as HTC-G. To clarify the effects of feedstocks on the ability of HTC, other samples were prepared with sucrose, fructose, or starch as the precursors and denoted as HTC-Su, HTC-F, and HTC-St, respectively.

To remove the oxygen-containing functional groups on the surface,[41] the HTC-G powders were thermally treated at three different temperatures (300, 500, and 700 °C) under a constant flow of argon gas. Typically, 0.5 g of the HTC-G sample was heated to 300 °C at a rate of 10 °C min^{-1} under an Ar flow for 3 h to obtain a sample denoted as HTC-300. The same procedure was repeated at higher temperatures of 500 and 700 °C to produce samples labeled as HTC-500 and HTC-700, respectively.

Earlier, there were reports that $NaBH_4$ could reduce carbonyl groups into hydroxyl groups[42] and that NaOH treatment could remove the hydroxyl groups on the surface of carbon materials.[43] Hence, in this work, $NaBH_4$ was used to change the number of carbonyl groups, and NaOH was used to reduce hydroxyl groups on the HTC surface. The $NaBH_4$ and NaOH treatments of HTC-G were

DOI: 10.1021/acsami.7b03310
ACS Appl. Mater. Interfaces 2017, 9, 17115−17124

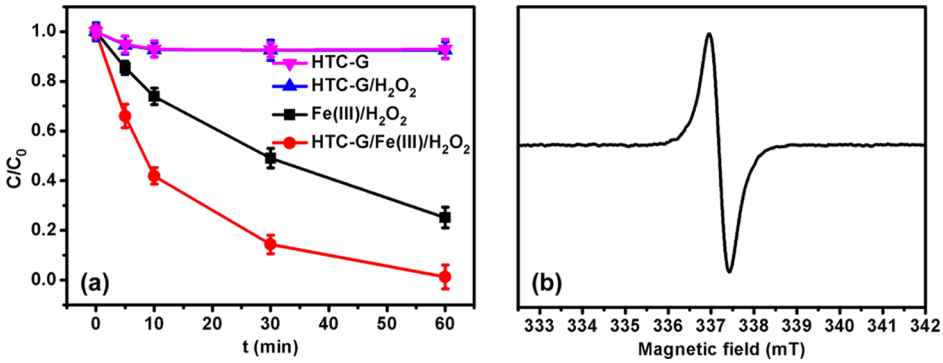

Figure 1. (a) Time profiles of the alachlor degradation in different systems. The initial concentrations of HTC-G, alachlor, Fe(III), and H_2O_2 are 0.25 g/L, 20 mg/L, 0.4 mmol/L, and 4 mmol/L, respectively. The initial pH value of the systems is 4.2; (b) ESR spectra of 0.01 g HTC-G particles.

performed as follows: 0.1 g of HTC-G was dispersed in 50 mL of $NaBH_4$ (1.6 mol/L) or NaOH (0.4 mol/L) solutions, and then, the mixture was stirred for 12 h or 24 h at room temperature. Finally, the products were collected by centrifugation and washed with deionized water and ethanol thoroughly and dried in vacuum at 60 °C for 24 h. The obtained samples were named as HTC-B and HTC-N.

2.3. Degradation Experiments of Alachlor. All of the experiments were performed in a 25 mL conical flask with continuous shaking on a rotary shaker (HY-5, China) at room temperature and normal pressure (Scheme S1). Typically, 5 mg of HTC was added into 20 mL of 20 mg/L alachlor aqueous solution (pH = 6.8), and the pH value of the solution did not change. Then, 200 μL of 0.04 mol/L Fe(III) was added into the solution, and the pH value decreased from 6.8 to 4.2. Finally, 80 μL of 1 mol/L H_2O_2 was added to trigger the degradation experiments. The pH value of the system did not adjust because Fe(III) was easy to precipitate at near neutral or basic pH. The degradation solutions were sampled out with a syringe at regular intervals and filtered immediately through a 0.22 μm nylon syringe filter to remove HTC-G. Ethanol (200 μL) was added immediately into 1 mL of the sample solution to quench the reaction for subsequent analysis.

2.4. Analytical Methods. Ferrous ion concentration was measured using a modified method using 1,10-phenanthroline with a UV−vis spectrophotometer (UV-2550, Shimadzu, Japan),[44] and benzoic acid was used as the probe for $^{\bullet}OH$ detection. The reaction of benzoic acid with hydroxyl radicals could produce three isomers of hydroxybenzoic acid with the ortho, meta, and para isomers in the ratio of 1.7:2.3:1.2.[45] The produced *para*-hydroxybenzoic acid (*p*-HBA) was quantified using high-pressure liquid chromatography. Scanning electron microscopy (SEM) was performed using a LEO 1450VP scanning electron microscope, and transition electron microscopy (TEM) was recorded on a JEOL-2100F microscope. Nitrogen adsorption−desorption isotherm was carried out on a Micromeritics Tristar-3000 surface area. The Brunauer−Emmett−Teller (BET) surface area was calculated from the linear part of the BET plot. The (*p*-hydroxyphenyl) acetic acid (POHPAA) fluorescence method was used to determine the concentration of H_2O_2 using a FluoroMax-4 spectrophotometer.[46] The fluorescence reagent was prepared by dissolving 1 mg of horseradish peroxidase and 2.7 mg of POHPAA in 10 mL of 8.2 g/L potassium hydrogen phthalate buffer solution. Typically, 200 μL of the sample and 50 μL of the fluorescence reagent were added to 2 mL of water. After 10 min, 1 mL of 0.1 mol/L NaOH solution was added to measure the intensity of the fluorescence emission at 409 nm excited at 315 nm. The concentration of alachlor was monitored using HPLC with an Agilent TC-C18 reverse-phase column (4.6 mm × 150 mm; Agilent, USA). The injection volume was set at 10 μL, and the mixture of 0.15% (w/w) acetic acid and acetonitrile (40/60, v/v) was used as the mobile phase with a flow rate of 1 mL/min, and the detection wavelength was set at 225 nm. The total organic carbon (TOC) was determined using a Shimadzu TOC-V CPH analyzer.

ESR spectra for radical determination in the HTC solution were recorded on a Bruker ESR A300 spectrometer. ATR−FTIR analyses were performed in the 4000−525 cm^{-1} region using a Nicolet iS50 FTIR spectrometer (Thermo).

3. RESULTS AND DISCUSSION

As shown in the SEM and TEM images, HTC-G consisted of uniform nanospheres with diameters of 200−300 nm and a core−shell structure (Figure S1), which are consistent with the published literature.[47,48] The adsorption and degradation curves of alachlor in different systems with an initial pH of 4.2 are shown in Figure 1a. It was found that only 7.5% of alachlor could be removed in the presence of HTC-G with the concentration of 0.25 g/L, suggesting a slight alachlor adsorption onto HTC-G. Meanwhile, with the addition of H_2O_2, the removal efficiency of alachlor (7.5%) remained unchanged, indicating that HTC-G could not directly decompose H_2O_2 to produce reactive species for alachlor degradation. However, about 74.8% of alachlor was degraded in Fe(III)/H_2O_2 system within 60 min, and the alachlor degradation efficiency increased to 98.7% when HTC-G of 0.25 g/L concentration was added into the HTC-G/Fe(III)/H_2O_2 Fenton-like system, suggesting that the presence of HTC-G could effectively enhance the alachlor degradation efficiency in the Fe(III)/H_2O_2 system. Both the alachlor degradation curves in Fe(III)/H_2O_2 and HTC-G/Fe(III)/H_2O_2 systems were found to fit the pseudo-first-order kinetics equations (Figure S2). The apparent alachlor degradation rate constant (k_{obs}) in the HTC-G/Fe(III)/H_2O_2 system (7.02×10^{-2} min^{-1}) was about 3 times higher than that of the Fe(III)/H_2O_2 system (2.25×10^{-2} min^{-1}) (Table S1). Meanwhile, the concentration changes of H_2O_2 in the Fe(III)/H_2O_2 and HTC-G/Fe(III)/H_2O_2 systems were also monitored. The concentrations of H_2O_2 in both the systems decreased slightly along with the increase in the reaction time (Figure S3) because of the overdose of H_2O_2. However, the consumption of H_2O_2 in the HTC-G/Fe(III)/H_2O_2 system was obviously higher than that in the Fe(III)/H_2O_2 system, indicating that the presence of HTC-G could enhance the decomposition of H_2O_2. This enhancement efficiency might be attributed to the direct interaction of HTC-G with Fe(III) ions because the classic homogeneous Fenton and Fenton-like reactions often suffer from the rapid precipitation of ferric ion and the unsatisfactory Fe(III)/Fe(II) cycle.

It has been well-established recently that carbonaceous materials contained different types of PFRs because of the unpaired π-electrons delocalizing over the aromatic rings.[49,50]

DOI: 10.1021/acsami.7b03310
ACS Appl. Mater. Interfaces 2017, 9, 17115−17124

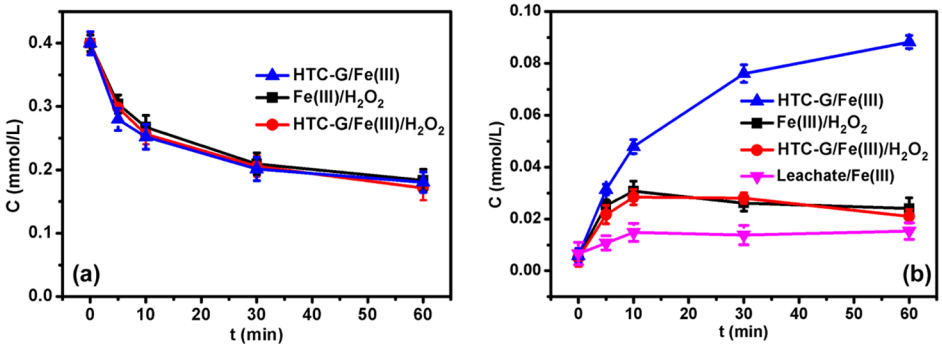

Figure 2. Variation in iron ion concentration in different systems during alachlor degradation: (a) total iron ions and (b) Fe(II) ions. The initial concentrations of HTC-G, Fe(III), and H_2O_2 are 0.25 g/L, 0.4 mmol/L, and 4 mmol/L, respectively. The initial pH value of the systems is 4.2.

The reference shows that the spectral splitting factor of ESR spectra (*g*-factor) was less than 2.0030 for carbon-centered PFRs without being connected with other heteroatoms; the *g*-factor was obtained in the range of 2.0030−2.0040 when carbon-centered PFRs were connected with an adjacent oxygen atom; and the *g*-factor was larger than 2.0040 for oxygen-centered PFRs.[51] For our results, the broad singlet signal was obtained with a *g*-factor of 2.0016 in the ESR spectra, and then, the existence of carbon-centered PFRs was confirmed for dried HTC-G powders (as shown in Figure 1b). Moreover, another reference was reported in which HTC that contained abundant quinone could uptake and release electrons through the conjugated π-electron systems.[52] Thus, in summary, the carbon-centered PFRs on the surface of HTC-G might act as an electron donor, transferring electrons from HTC-G to the electron acceptor, namely, Fe(III) ions, to produce Fe(II) ions and to significantly improve the degradation efficiencies of alachlor in HTC-G/Fe(III)/H_2O_2 Fenton-like systems.

Therefore, the concentration changes of the total dissolved iron and Fe(II) ions in different systems were monitored. The concentrations of total dissolved iron ions in the Fe(III)/H_2O_2, HTC-G/Fe(III), and HTC-G/Fe(III)/H_2O_2 systems were found to decrease significantly with the reaction time (as shown in Figure 2a), revealing that the presence of HTC-G could not maintain iron in soluble forms. Due to the weak reduction ability of H_2O_2 to reduce Fe(III) to Fe(II), the concentration of Fe(II) ions in the Fe(III)/H_2O_2 system was very low (Figure 2b). However, the concentration of Fe(II) ions increased gradually in the HTC-G/Fe(III) system, confirming that HTC-G could enhance the reduction of Fe(III) ions to Fe(II) ions. Fe(II) ion concentration change curve in the HTC-G/Fe(III)/H_2O_2 system was similar to that of the Fe(III)/H_2O_2 system, which may be attributed to the difference in the rapid consumption of Fe(II) ions through the Fenton reaction from the reduction of Fe(III) ions. To further probe the original electron transfer and the reduction ability of HTC-G/Fe(III) and HTC-G/Fe(III)/H_2O_2 systems, the concentration changes of Fe(II) ions in the solution of HTC-G particles and in the leachates from these HTC-G particles were compared. As shown in Figure 2b, the concentration of Fe(II) ions was very low, and no reduction happened when Fe(III) ions were added into the leachates of HTC-G. These results indicated that the leachates of HTC-G could not reduce Fe(III) to Fe(II). Thus, it can be confirmed that the reduction of Fe(III) to Fe(II) occurred on the surface of HTC-G rather than in the leachates.

Subsequently, to clarify the factors affecting the reduction ability of HTC-G, four kinds of HTC, synthesized under the same conditions with different organic precursors (glucose, sucrose, fructose, or starch), were attempted to check the influences of carbon precursors. The specific surface areas of the four HTC samples were analyzed using the BET nitrogen adsorption technique, and the results were obtained as 31.0, 21.5, 37.1, and 19.1 $m^2 \cdot g^{-1}$ (Table S1). The ATR−FTIR examination revealed that a considerable number of functional groups can be observed from all four HTC samples (Figure S4a). The peaks at 2972, 2928, and 1361 cm^{-1} were ascribed to the stretching vibration of the C−H bond. The peaks at 1699 and 1608 cm^{-1} were attributed to C═O and C═C vibrations. The peaks at 3000−3600 and 1000−1300 cm^{-1} were assigned to the O−H stretching vibration and C−OH bending vibrations. No significant functional group differences were observed from the four different prepared HTC samples. The effects of carbon precursors on the formed PFRs with different prepared HTC samples were also examined using ESR spectroscopy (Figure S4b). The *g*-factors were obtained as 2.0016, 2.0015, 2.0016, and 2.0015 for HTC-G, HTC-Su, HTC-F, and HTC-St, respectively, confirming the existence of carbon-centered PFRs, and no PFR difference was observed for the four different prepared HTC samples. However, the peak intensities of the carbon-centered PFRs in HTC were significantly influenced by the carbon precursors. The ESR peak intensity of HTC samples was in the order of HTC-Su > HTC-St > HTC-G > HTC-F. However, the concentration changes of the total dissolved iron and Fe(II) ions were almost the same in HTC/Fe(III) systems with four kinds of HTC (Figure S5). These results suggested that the carbon precursors might not be the main factor affecting the reduction ability of HTC.

To further understand the contribution of different HTC samples prepared from the four carbon precursors to the degradation of alachlor in the HTC/Fe(III)/H_2O_2 system, the degradation efficiencies of the four systems were also compared. As shown in Figure S5c, 98.7, 98.7, 96.4, and 92.6% of alachlor were degraded within the same time intervals of 60 min in HTC-G/Fe(III)/H_2O_2, HTC-Su/Fe(III)/H_2O_2, HTC-F/Fe(III)/H_2O_2, and HTC-St/Fe(III)/H_2O_2 systems, respectively, and the corresponding k_{obs} were obtained as 7.02 × 10^{-2}, 7.15 × 10^{-2}, 5.33 × 10^{-2}, and 4.18 × 10^{-2} min^{-1} (Figure S5d). It is well-known that the surface area could affect the reactivity of the catalyst; therefore, the BET surface areas of the four samples were also measured, and the k_{obs} values normalized with the specific surface area (k_{surf}) were calculated

DOI: 10.1021/acsami.7b03310
ACS Appl. Mater. Interfaces 2017, 9, 17115−17124

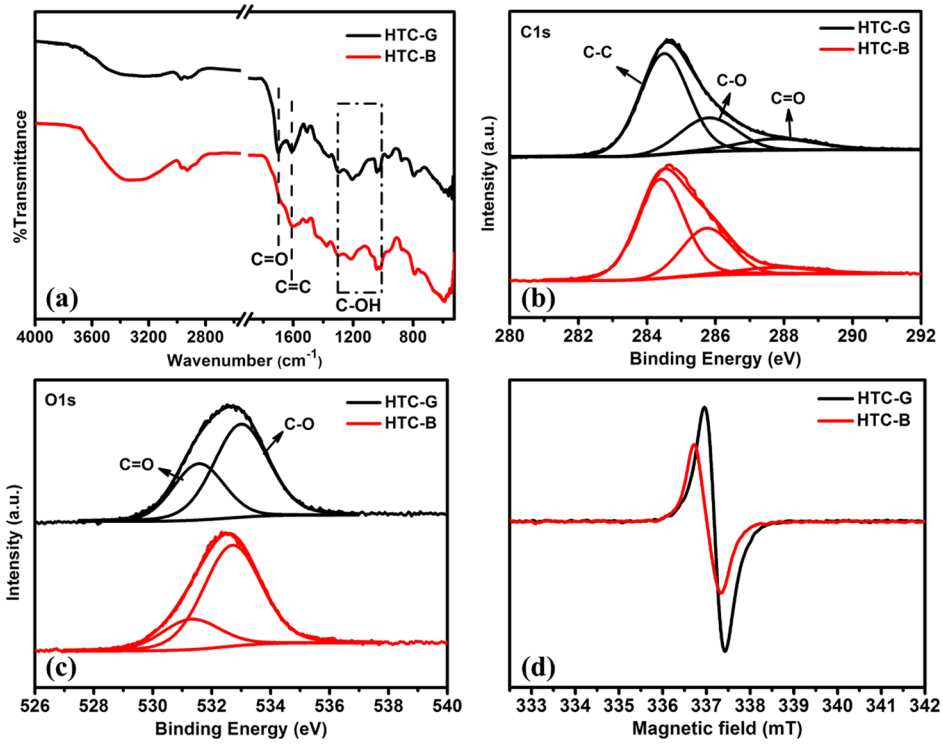

Figure 3. (a) ATR−FTIR spectra of HTC-B and HTC-G; high-resolution spectra of (b) C 1s and (c) O 1s within XPS spectra of HTC-B and HTC-G; and (d) ESR spectra of 0.01 g HTC-B and HTC-G particles.

to be 2.26×10^{-3}, 2.16×10^{-3}, 2.37×10^{-3}, and 2.19×10^{-3} $m^2 \cdot g^{-1} \cdot min^{-1}$ for these four systems (Table S1). Thus, these results indicate that the carbon precursors do not significantly influence the reduction ability of HTC and the degradation efficiencies of alachlor, though it can slightly affect the BET surface area of HTC.

As discussed above, the reduction of Fe(III) ions occurred on the surface of HTC; hence, the influences of the surface properties on the reduction ability of HTC were also investigated. First, a thermal treatment under Ar was applied to remove the surface functional groups on HTC-G, and the SEM observations showed that all of HTC-G samples before and after the thermal treatment at different temperatures consisted of uniform nanospheres with diameters of 200−300 nm (Figure S6a), revealing that the thermal treatment did not change the morphology of HTC-G. ATR−FTIR spectra indicated that the infrared absorption intensity of the peaks at 3000−3600, 1699, and 1000−1300 cm^{-1} for HTC-G, HTC-300, and HTC-500, respectively, corresponding to the hydroxyl and carbonyl groups, decreased significantly along with the increase in the treatment temperature from 0 to 500 °C (Figure S6b). When the treatment temperature increased to 700 °C, the infrared absorption intensity of all peaks of the surface functional groups including −OH and C═O almost disappeared. These results demonstrated that the thermal treatment under Ar could effectively remove the surface functional groups on HTC. Subsequently, the concentration changes of total dissolved iron and Fe(II) ions in the four HTC/Fe(III) systems were monitored to evaluate the influences of surface functional groups on the reduction ability of HTC, and the concentration changes of total iron ions in the HTC-300/Fe(III), HTC-500/Fe(III), and HTC-700/Fe(III) systems were almost the same as that in the HTC-G/Fe(III) system (Figure S7a), indicating that HTC before and after thermal treatment at different temperatures does not change the concentration of total iron ions. However, with the increasing temperature from without treatment to 700 °C, the concentration of Fe(II) ions first increases slightly in the HTC-300/Fe(III) system and then dramatically decreases in the HTC-500/Fe(III) and HTC-700/Fe(III) systems, even lower than that in the HTC-G/Fe(III) system (Figure S7b). The slight increase in the concentration of Fe(II) ions in the HTC-300/Fe(III) system might be attributed to the partial carbonization of organic molecules and the formation of some functional groups on the surface of HTC-G.[53,54]

Similarly, the overall degradation efficiencies of alachlor also slightly increase from 98.7 to 99.7% for HTC-G and then rapidly decrease to 94.5 and 90.0% (Figure S7c) when the treatment temperature is increased from 300 to 700 °C. The k_{obs} values in the four HTC/Fe(III)/H_2O_2 systems were calculated to be 7.02×10^{-2}, 7.35×10^{-2}, 4.64×10^{-2}, and 3.69×10^{-2} min^{-1} (Figure S7d). These results confirm that the surface functional groups on HTC play an important role in the electron transfer from HTC to Fe(III) ions and in the degradation efficiencies of alachlor.

To further clarify the surface functional groups, the $NaBH_4$ treatment was first used to reduce carbonyl groups into hydroxyl groups, and the ATR−FTIR spectra of HTC-G were used to monitor the evolution of functional groups. Figure 3a shows that the peak at 1699 cm^{-1} corresponding to the carbonyl group stretching vibration decreased distinctly, and the peak between 3000 and 3600 cm^{-1} assigned to O−H stretching vibrations increased after $NaBH_4$ treatment. The results were further confirmed using X-ray photoelectron spectroscopy (XPS) analysis. The high-resolution C 1s peak of HTC could be fitted by three peaks at the binding energies of 284.5, 285.8, and 287.8 eV, which were assigned to C−C, C−OH, and C═O (Figure 3b), respectively, further

DOI: 10.1021/acsami.7b03310
ACS Appl. Mater. Interfaces 2017, 9, 17115−17124

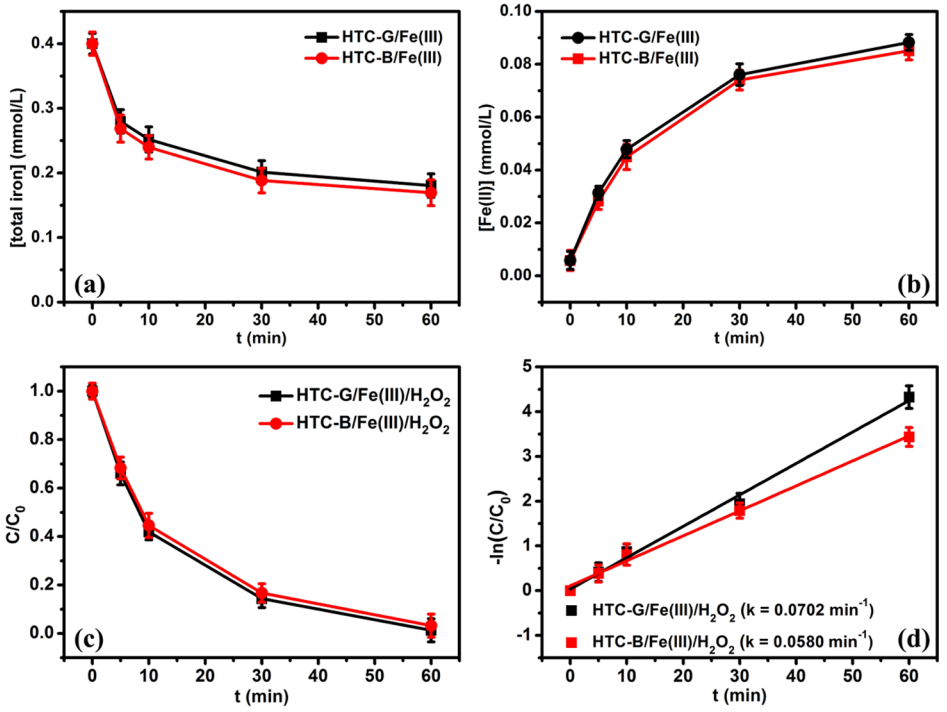

Figure 4. Variation in iron ion concentration in different systems during alachlor degradation: (a) Fe(II) ions and (b) total iron ions. (c) Time profiles of alachlor degradation in different systems; (d) plots of $-\ln(C/C_0)$ vs time for alachlor degradation in different systems. The initial concentrations of HTC, alachlor, Fe(III), and H_2O_2 are 0.25 g/L, 20 mg/L, 0.4 mmol/L, and 4 mmol/L, respectively. The initial pH value of the systems is 4.2.

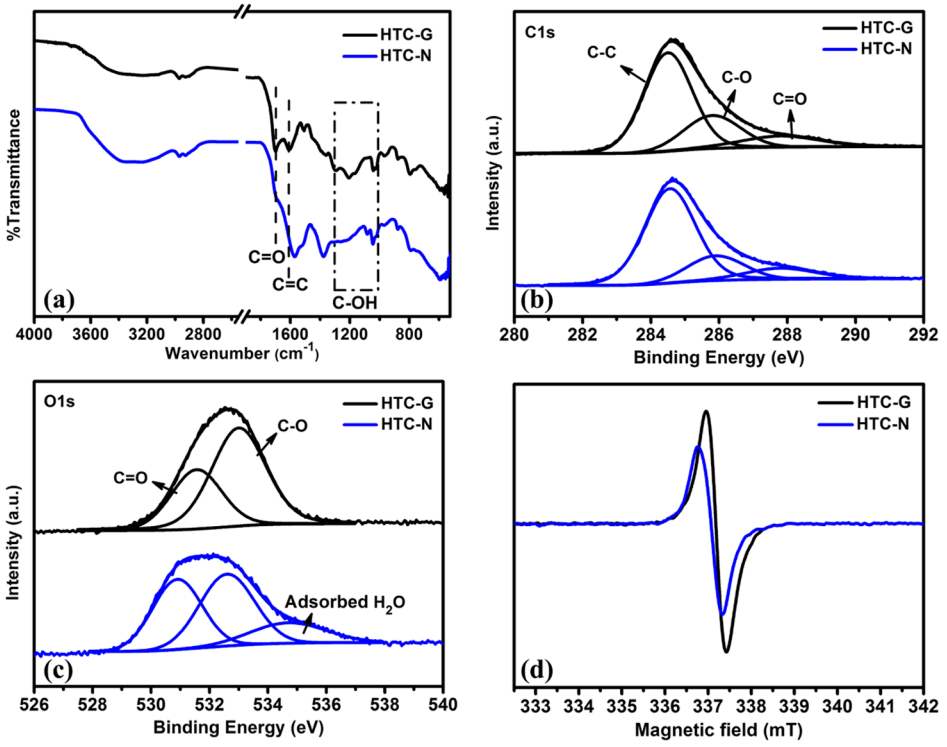

Figure 5. (a) ATR-FTIR spectra of HTC-N and HTC-G; high-resolution spectra of (b) C 1s and (c) O 1s within XPS spectra of HTC-N and HTC-G; and (d) ESR spectra of 0.01 g HTC-N and HTC-G particles.

confirming the existence of abundant oxygen-containing functional groups, for example, hydroxyl and carbonyl groups, on the surface of HTC. Meanwhile, the ratio of carbon in the hydroxyl groups to total carbon (C_{C-OH}/C_{total}), and the ratio of carbon in the carbonyl groups to total carbon ($C_{C=O}/C_{total}$) were also calculated from the peak areas in the C 1s spectra. It was found that the C_{C-OH}/C_{total} ratio increased from 23.7% (HTC-G) to 29.5% (HTC-B), whereas the $C_{C=O}/C_{total}$ ratio

DOI: 10.1021/acsami.7b03310
ACS Appl. Mater. Interfaces 2017, 9, 17115−17124

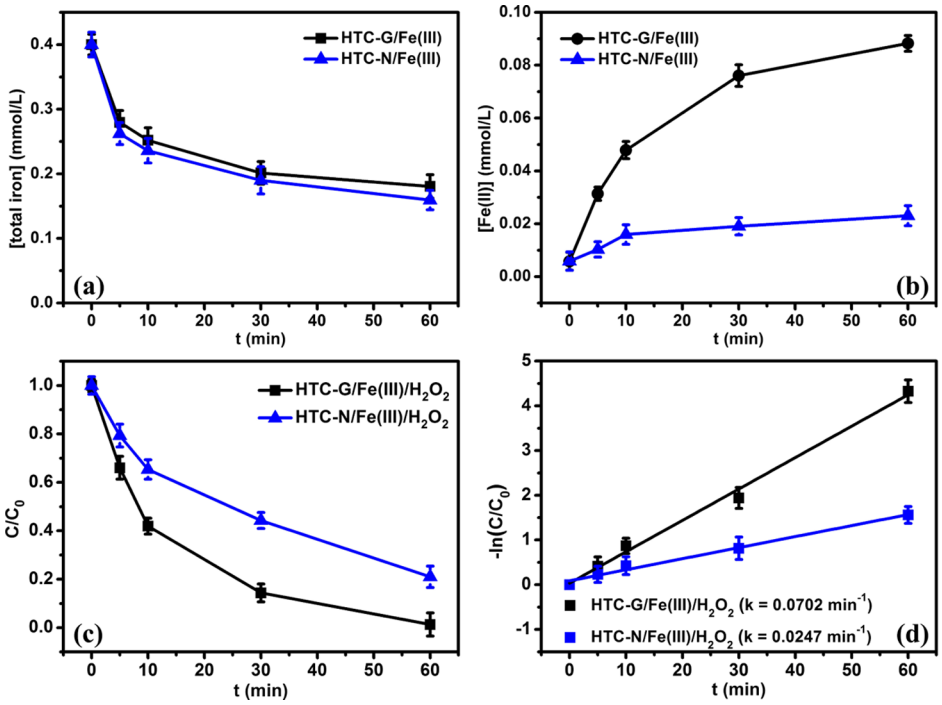

Figure 6. Variation in iron ion concentration in different systems during alachlor degradation: (a) Fe(II) ions and (b) total iron ions; (c) time profiles of alachlor degradation in different systems; (d) plots of $-\ln(C/C_0)$ vs time for alachlor degradation in different systems. The initial concentrations of HTC, alachlor, Fe(III), and H_2O_2 are 0.25 g/L, 20 mg/L, 0.4 mmol/L, and 4 mmol/L, respectively. The initial pH value of the systems was 4.2.

decreased from 12.5% (HTC-G) to 7.5% (HTC-B) after $NaBH_4$ treatment (Table S2), suggesting that $NaBH_4$ treatment could effectively reduce carbonyl groups on the HTC-G surface into hydroxyl groups. Similar results were also obtained in the O 1s spectra of HTC-G and HTC-B (Figure 3b), which could be decomposed into two peaks at the binding energies of 531.5 (C═O) and 533 eV (C−OH), respectively. The ratio of oxygen in the hydroxyl groups to total oxygen (O_{C-OH}/O_{total}) increased from 64.9% (HTC-G) to 77.0% (HTC-B), whereas the ratio of oxygen in the carbonyl groups to total oxygen ($O_{C=O}/O_{total}$) decreased from 35.1% (HTC-G) to 23.0% (HTC-B) after $NaBH_4$ treatment (Table S2), in agreement with the variation trend of the C_{C-OH}/C_{total} and $C_{C=O}/C_{total}$ ratios. Then, ESR spectra were also used to compare the radical types and radical concentrations in HTC before and after $NaBH_4$ treatment (Figure 3d), and the *g*-factors were obtained as 2.0016 and 2.0026 for HTC-G and HTC-B, respectively, suggesting that the carbon-centered PFRs still remained, although the data have a slight shift after $NaBH_4$ treatment. Furthermore, the ESR signal of HTC-B was greatly lower than that of HTC-G, indicating that the concentration of carbon-centered PFRs is much lower in HTC-B than in HTC-G.

Subsequently, the concentration changes of total iron ions and dissolved Fe(II) in the HTC-B/Fe(III) system were monitored, and the relative results are shown in Figure 4a,b. The data are almost the same as that of the HTC-G/Fe(III) system, suggesting that the carbonyl groups on the surface of HTC may not significantly affect the reduction ability of HTC. To further confirm these results, the alachlor degradation in the HTC-B/Fe(III)/H_2O_2 system was also compared (Figure 4c). The k_{obs} values were calculated to be 5.80×10^{-2} and 2.47×10^{-2} in the systems with HTC-B and HTC-G, respectively (Figure 4d and Table S1). The normalized rate constant, k_{surf}, over HTC-G and HTC-B were calculated to be 2.27×10^{-3} and 2.03×10^{-3} $m^2 \cdot g^{-1} \cdot min^{-1}$, respectively, because the BET surface area decreased from 31.0 $m^2 \cdot g^{-1}$ (HTC-G) to 28.5 $m^2 \cdot g^{-1}$ (HTC-B) after $NaBH_4$ treatment. That is, k_{surf} with HTC was not significantly influenced by the $NaBH_4$ treatment. On the basis of these results, it was concluded that the carbonyl groups on the HTC surface were not the main factors affecting its reactivity.

Also, the NaOH treatment was performed to change the number of hydroxyl groups on the HTC surface, and FTIR spectra was used to check the evolution of this functional group. The results indicated that the characteristic peaks of hydroxyl groups at 1000−1300 cm^{-1} decreased significantly, but the peaks at 3000−3600 cm^{-1} increased obviously after the NaOH treatment, as shown in Figure 5a. The high-resolution spectra of XPS also revealed that the O/C ratios of HTC-N after the NaOH treatment (36.6%) were higher than those of HTC-G (34.7%), though the C_{C-OH}/C_{total} (20.0%) and $C_{C=O}/C_{total}$ (11.1%) ratios of HTC-N were slightly lower than those of HTC-G (Figure 5b and Table S2). To clarify these results, further analysis of the high-resolution spectra of O 1s was also conducted. In comparison with HTC-G, a new peak appeared at 535.2 eV in HTC-N (Figure 5c), which was assigned to adsorbed water, attributed to the increase in the O/C ratio in HTC-N. The O_{C-OH}/O_{total} in HTC-N (43.9%) was apparently lower than that in HTC-G (64.9%) (Table S2), indicating that the NaOH treatment can effectively remove the hydroxyl groups on the surface of HTC-G. The ESR spectra in Figure 5d show that the *g*-factors of HTC-G and HTC-N were obtained as 2.0016 and 2.0023, respectively, suggesting that the NaOH treatment also did not change the types of carbon-centered PFRs of HTC.

The concentrations of total iron and Fe(II) ions in HTC-B/Fe(III) systems were further detected, and it was found that the total iron ion concentration decreased gradually with the

DOI: 10.1021/acsami.7b03310
ACS Appl. Mater. Interfaces 2017, 9, 17115−17124

reaction time (Figure 6a) and almost the same as that of the HTC-G/Fe(III) system, but Fe(II) ion concentration in the HTC-N/Fe(III) system was significantly lower than that of the HTC-G/Fe(III) system (Figure 6b). These results indicate that the hydroxyl groups on the surface of HTC may strongly affect the reduction ability of HTC. Then, the degradation efficiencies of alachlor in the HTC-N/Fe(III)/H_2O_2 system were investigated to confirm these results. As shown in Figure 6c, the alachlor degradation efficiency in HTC-N/Fe(III)/H_2O_2 system was obtained as 78.9% and k_{obs} was obtained as 2.47 × 10^{-2} min^{-1} within 60 min (Figure 6d). Also, k_{surf} with HTC-N was obtained as 4.97 × 10^{-4} $m^2 \cdot g^{-1} \cdot min^{-1}$ (Table S2), which was greatly lower than that of HTC-G (without NaOH treatment) of 2.27 × 10^{-3} $m^2 \cdot g^{-1} \cdot min^{-1}$. The change in the trends of k_{surf} of HTC before and after NaOH treatment was consistent with the reduction potential of HTC. On the basis of these results, it can be concluded that the hydroxyl groups were mainly responsible for the electron transfer from HTC to Fe(III) ions.

It is also well-known that Fe(II) ions could catalytically decompose H_2O_2 to produce •OH through the Fenton reaction. Therefore, benzoic acid was used to identify the •OH concentration in both Fe(III)/H_2O_2 and HTC-G/Fe(III)/H_2O_2 systems (Figure S8a). The cumulative •OH in both the systems were achieved as 0.15 and 0.45 mmol/L, well-matched with the degradation trend of alachlor. The presence of HTC-G could significantly improve the catalytic recycle of Fe(II) ions and then enhance the •OH concentration and the degradation efficiencies of alachlor in the HTC-G/Fe(III)/H_2O_2 system. Isopropanol was also used in this work as an •OH scavenger to probe the contribution of •OH to alachlor degradation. As shown in Figure S8b, the addition of isopropanol completely inhibited alachlor degradation, confirming that •OH was mainly responsible for alachlor degradation in the HTC-G/Fe(III)/H_2O_2 system. Thus, it can be concluded that the addition of HTC-G did not change the type of reactive oxygen species within this Fenton-like system but significantly promoted the redox cycle of Fe(III)/Fe(II) in the HTC-G/Fe(III)/H_2O_2 system.

The stability of catalysts is also a key issue for their practical application. Therefore, the used HTC-G were cleaned with deionized water and then reused six times for the degradation of alachlor within the HTC-G/Fe(III)/H_2O_2 system under the same conditions. It was interesting to find that no obvious decrease in the activity of HTC-G catalysts was observed in the degradation efficiencies of alachlor after seven recycles, suggesting that this carbonaceous catalyst has good reusability and has great potential in their practical application (Figure 7). Then, we compared the ATR−FTIR and XPS spectra of HTC-G before (HTC-G) and after the Fenton-like process (reclaimed HTC-G) and found that there were no significant differences between the functional groups on the surface of HTC-G and reclaimed HTC-G (Figures S9 and S10). The C_{C-OH}/C_{total} ratio decreased from 23.7% (HTC-G) to 22.4% (reclaimed HTC-G), whereas the $C_{C=O}/C_{total}$ ratio increased from 12.5% (HTC-G) to 13.6% (reclaimed HTC-G) (Table S2). Similarly, the O_{C-OH}/O_{total} ratio in reclaimed HTC-G (63.1%) was slightly lower than that in HTC-G (64.9%), and the $O_{C=O}/O_{total}$ ratio in reclaimed HTC-G (36.9%) was slightly lower than that in HTC-G (35.1%) (Table S2). However, the high-resolution spectra of Fe 2p (Figure S7c) indicated that a certain amount of iron oxide was adsorbed on the surface of reclaimed HTC-G.

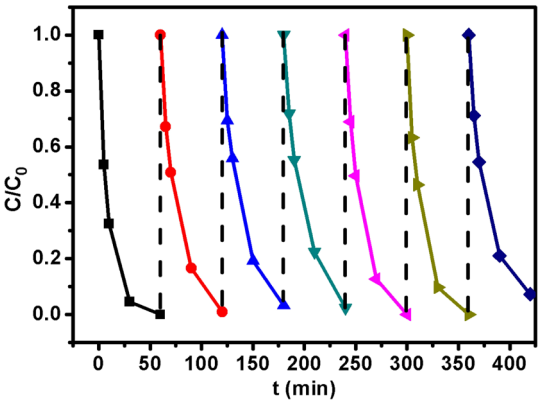

Figure 7. Recycling experiments of HTC-G for alachlor degradation in HTC-G/Fe(III)/H_2O_2 system. The initial concentrations of HTC-G, alachlor, Fe(III), and H_2O_2 are 0.25 g/L, 20 mg/L, 0.4 mmol/L, and 4 mmol/L, respectively. The initial pH value of the systems is 4.2.

On the basis of the above results and analyses, a possible degradation mechanism was proposed to explain the HTC-promoted alachlor degradation in the HTC/Fe(III)/H_2O_2 Fenton-like system (Scheme 1). First, Fe(III) ions were

Scheme 1. Schematic Diagram for HTC-Enhanced Degradation of Alachlor via Fenton-Like Reaction

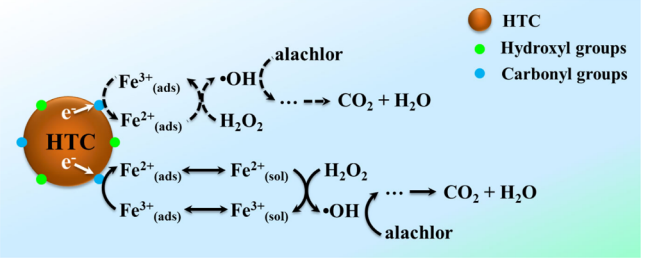

adsorbed onto the surface of HTC and form complexes with the hydroxyl groups on the HTC surface. Second, electron transfer from HTC to Fe(III) occurred, and the reduction of Fe(III) ions to Fe(II) ions happened. Third, Fe(II) ions reacted with H_2O_2 to catalytically produce •OH quickly. That is, the presence of HTC-G effectively enhanced the Fe(III)/Fe(II) cycle to maintain enough Fe(II) ions in this Fenton-like system and thus favor the fast catalytic decomposition of H_2O_2 to produce highly reactive •OH for the degradation and final decontamination of alachlor. TOC analysis was also monitored to probe the mineralization and the fate of alachlor in different systems (Figure S11). The control experiments indicated that a negligible removal of TOC was observed in HTC-G/Fe(III) system because only a small amount of alachlor was adsorbed by HTC-G particles. However, in the degradation system, about 30.6 and 41.6% of alachlor were mineralized in Fe(III)/H_2O_2 and HTC-G/Fe(III)/H_2O_2 systems, respectively, within 8 h. This comparison revealed that the presence of HTC-G can not only significantly increase the degradation but also enhance the mineralization efficiencies of alachlor in this Fenton-like system.

4. CONCLUSIONS

In this study, we find that the presence of HTC could effectively promote the degradation of alachlor in the Fe(III)/H_2O_2 Fenton-like system by realizing the efficient Fe(III)/

DOI: 10.1021/acsami.7b03310
ACS Appl. Mater. Interfaces 2017, 9, 17115−17124

Fe(II) cycle. HTC transferred the electron to Fe(III) ions, which could form complexes with the hydroxyl groups on the surface of HTC to produce Fe(II) ions and thus favored the H_2O_2 decomposition to produce more hydroxyl radicals for the alachlor degradation. For its good stability, HTC can be reused and hence avoid the possible adverse environmental consequences caused by soluble compounds. It is well-known that H_2O_2 and Fe(III) are ubiquitous in natural water environments; in spite of the tiny amount, the widely present carbon materials may promote the transformation of POPs via Fe(III)/H_2O_2 Fenton reaction. Our findings here provide a new insight into the potential role of carbon materials on the transformation of POPs via Fenton oxidation processes.

Although we have demonstrated that PFRs in HTC can act as an electron donor to transfer electrons from HTC-G to Fe(III), the transformation mechanism of PFRs in HTC has not been included in the present work. Moreover, HTC may also indirectly or directly react with contaminants through the abundant PFRs in the natural environment. Therefore, the formation and transformation mechanism of PFRs in HTC and the further reactions with contaminants would be studied in the future work to deeply understand the role of HTC in the migration and transformation of contaminants in the natural aquatic ecosystem.

■ ASSOCIATED CONTENT

Supporting Information

The Supporting Information is available free of charge on the ACS Publications website at DOI: 10.1021/acsami.7b03310.

Instrument of the alachlor degradation experiment; SEM and TEM images of HTC-G; plots of $-\ln(C/C_0)$ versus time for alachlor degradation; variation in H_2O_2 concentration; ATR−FTIR and ESR spectra of HTC; variation in iron ion and alachlor concentrations; SEM images and ATR−FTIR spectra of HTC-G before and after thermal treatment; variation in $^{\bullet}OH$ concentration and alachlor degradation in the presence of a scavenger; ATR−FTIR spectra of HTC-G before and after use; XPS spectra of HTC-G before and after use; TOC removal in different systems; summary of alachlor degradation constants, BET areas of HTC, and normalized degradation constants of alachlor; and elemental composition of different HTC samples (PDF)

■ AUTHOR INFORMATION

Corresponding Authors

*E-mail: zhanglz@mail.ccnu.edu.cn. Phone: +86-27-67867535 (L.Z.).

*E-mail: antc99@gdut.edu.cn. Phone: +86-20-23883536 (T.A.).

ORCID

Lizhi Zhang: 0000-0002-6842-9167

Taicheng An: 0000-0001-6918-8070

Notes

The authors declare no competing financial interest.

■ ACKNOWLEDGMENTS

This work was supported by the National Natural Science Funds for Distinguished Young Scholars (21425728 and 41425015), the National Science Foundation of China (21273088 and 21477044), and the Self-Determined Research Funds of CCNU from the Colleges' Basic Research and Operation of MOE (Grant CCNU14Z01001 and CCNU14K-FY002).

■ REFERENCES

(1) Dong, H.; Zeng, G.; Tang, L.; Fan, C.; Zhang, C.; He, X.; He, Y. An Overview on Limitations of TiO_2-Based Particles for Photocatalytic Degradation of Organic Pollutants and the Corresponding Countermeasures. *Water Res.* **2015**, *79*, 128−146.

(2) Yang, R.; Zhang, S.; Li, A.; Jiang, G.; Jing, C. Altitudinal and Spatial Signature of Persistent Organic Pollutants in Soil, Lichen, Conifer Needles, and Bark of the Southeast Tibetan Plateau: Implications for Sources and Environmental Cycling. *Environ. Sci. Technol.* **2013**, *47*, 12736−12743.

(3) Zhang, K.; Wei, Y.-L.; Zeng, E. Y. A Review of Environmental and Human Exposure to Persistent Organic Pollutants in the Pearl River Delta, South China. *Sci. Total Environ.* **2013**, *463−464*, 1093−1110.

(4) Guan, B. Y.; Yu, L.; Lou, X. W. A Dual-Metal−Organic-Framework Derived Electrocatalyst for Oxygen Reduction. *Energy Environ. Sci.* **2016**, *9*, 3092−3096.

(5) Stefaniuk, M.; Oleszczuk, P.; Ok, Y. S. Review on Nano Zerovalent Iron (nZVI): From Synthesis to Environmental Applications. *Chem. Eng. J.* **2016**, *287*, 618−632.

(6) Cho, D.-W.; Kwon, G.; Ok, Y. S.; Kwon, E. E.; Song, H. Reduction of Bromate by Cobalt-Impregnated Biochar Fabricated Via Pyrolysis of Lignin Using CO_2 as a Reaction Medium. *ACS Appl. Mater. Interfaces* **2017**, *9*, 13142−13150.

(7) Guinea, E.; Brillas, E.; Centellas, F.; Cañizares, P.; Rodrigo, M. A.; Sáez, C. Oxidation of Enrofloxacin with Conductive-Diamond Electrochemical Oxidation, Ozonation and Fenton Oxidation. A Comparison. *Water Res.* **2009**, *43*, 2131−2138.

(8) Wols, B. A.; Hofman-Caris, C. H. M. Review of Photochemical Reaction Constants of Organic Micropollutants Required for UV Advanced Oxidation Processes in Water. *Water Res.* **2012**, *46*, 2815−2827.

(9) Munoz, M.; de Pedro, Z. M.; Casas, J. A.; Rodriguez, J. J. Preparation of Magnetite-Based Catalysts and Their Application in Heterogeneous Fenton Oxidation—A Review. *Appl. Catal., B* **2015**, *176−177*, 249−265.

(10) Bokare, A. D.; Choi, W. Review of Iron-Free Fenton-Like Systems for Activating H_2O_2 in Advanced Oxidation Processes. *J. Hazard. Mater.* **2014**, *275*, 121−135.

(11) Cornelissen, G.; Haftka, J.; Parsons, J.; Gustafsson, Ö. Sorption to Black Carbon of Organic Compounds with Varying Polarity and Planarity. *Environ. Sci. Technol.* **2005**, *39*, 3688−3694.

(12) Ji, L.; Wan, Y.; Zheng, S.; Zhu, D. Adsorption of Tetracycline and Sulfamethoxazole on Crop Residue-Derived Ashes: Implication for the Relative Importance of Black Carbon to Soil Sorption. *Environ. Sci. Technol.* **2011**, *45*, 5580−5586.

(13) Teixidó, M.; Hurtado, C.; Pignatello, J. J.; Beltrán, J. L.; Granados, M.; Peccia, J. Predicting Contaminant Adsorption in Black Carbon (Biochar)-Amended Soil for the Veterinary Antimicrobial Sulfamethazine. *Environ. Sci. Technol.* **2013**, *47*, 6197−6205.

(14) Mohan, D.; Sarswat, A.; Ok, Y. S.; Pittman, C. U., Jr. Organic and Inorganic Contaminants Removal from Water with Biochar, a Renewable, Low Cost and Sustainable Adsorbent—A Critical Review. *Bioresour. Technol.* **2014**, *160*, 191−202.

(15) Fernandez, M. E.; Ledesma, B.; Román, S.; Bonelli, P. R.; Cukierman, A. L. Development and Characterization of Activated Hydrochars from Orange Peels as Potential Adsorbents for Emerging Organic Contaminants. *Bioresour. Technol.* **2015**, *183*, 221−228.

(16) Wu, Z.; Yuan, X.; Zhang, J.; Wang, H.; Jiang, L.; Zeng, G. Photocatalytic Decontamination of Wastewater Containing Organic Dyes by Metal-Organic Frameworks and Their Derivatives. *ChemCatChem* **2017**, *9*, 41−64.

(17) Saputra, E.; Muhammad, S.; Sun, H.; Wang, S. Activated Carbons as Green and Effective Catalysts for Generation of Reactive

DOI: 10.1021/acsami.7b03310
ACS Appl. Mater. Interfaces 2017, 9, 17115−17124

Radicals in Degradation of Aqueous Phenol. *RSC Adv.* **2013**, *3*, 21905−21910.
(18) Ribeiro, R. S.; Silva, A. M. T.; Figueiredo, J. L.; Faria, J. L.; Gomes, H. T. The Influence of Structure and Surface Chemistry of Carbon Materials on the Decomposition of Hydrogen Peroxide. *Carbon* **2013**, *62*, 97−108.
(19) Wang, Y.; Xie, Y.; Sun, H.; Xiao, J.; Cao, H.; Wang, S. Efficient Catalytic Ozonation over Reduced Graphene Oxide for P-Hydroxylbenzoic Acid (HBA) Destruction: Active Site and Mechanism. *ACS Appl. Mater. Interfaces* **2016**, *8*, 9710−9720.
(20) Fang, G.; Zhu, C.; Dionysiou, D. D.; Gao, J.; Zhou, D. Mechanism of Hydroxyl Radical Generation from Biochar Suspensions: Implications to Diethyl Phthalate Degradation. *Bioresour. Technol.* **2015**, *176*, 210−217.
(21) Fang, G.; Gao, J.; Liu, C.; Dionysiou, D. D.; Wang, Y.; Zhou, D. Key Role of Persistent Free Radicals in Hydrogen Peroxide Activation by Biochar: Implications to Organic Contaminant Degradation. *Environ. Sci. Technol.* **2014**, *48*, 1902−1910.
(22) Fang, G.; Liu, C.; Gao, J.; Dionysiou, D. D.; Zhou, D. Manipulation of Persistent Free Radicals in Biochar to Activate Persulfate for Contaminant Degradation. *Environ. Sci. Technol.* **2015**, *49*, 5645−5653.
(23) Kappler, A.; Wuestner, M. L.; Ruecker, A.; Harter, J.; Halama, M.; Behrens, S. Biochar as an Electron Shuttle between Bacteria and Fe(III) Minerals. *Environ. Sci. Technol. Lett.* **2014**, *1*, 339−344.
(24) Klüpfel, L.; Keiluweit, M.; Kleber, M.; Sander, M. Redox Properties of Plant Biomass-Derived Black Carbon (Biochar). *Environ. Sci. Technol.* **2014**, *48*, 5601−5611.
(25) Xiao, L.-P.; Shi, Z.-J.; Xu, F.; Sun, R.-C. Hydrothermal Carbonization of Lignocellulosic Biomass. *Bioresour. Technol.* **2012**, *118*, 619−623.
(26) Qian, K.; Kumar, A.; Zhang, H.; Bellmer, D.; Huhnke, R. Recent Advances in Utilization of Biochar. *Renewable Sustainable Energy Rev.* **2015**, *42*, 1055−1064.
(27) Tekin, K.; Karagöz, S.; Bektaş, S. A Review of Hydrothermal Biomass Processing. *Renewable Sustainable Energy Rev.* **2014**, *40*, 673−687.
(28) Falco, C.; Baccile, N.; Titirici, M.-M. Morphological and Structural Differences between Glucose, Cellulose and Lignocellulosic Biomass Derived Hydrothermal Carbons. *Green Chem.* **2011**, *13*, 3273−3281.
(29) Liu, Z.; Balasubramanian, R. Upgrading of Waste Biomass by Hydrothermal Carbonization (HTC) and Low Temperature Pyrolysis (LTP): A Comparative Evaluation. *Appl. Energy* **2014**, *114*, 857−864.
(30) Möller, M.; Nilges, P.; Harnisch, F.; Schröder, U. Subcritical Water as Reaction Environment: Fundamentals of Hydrothermal Biomass Transformation. *ChemSusChem* **2011**, *4*, 566−579.
(31) Kambo, H. S.; Dutta, A. A Comparative Review of Biochar and Hydrochar in Terms of Production, Physico-Chemical Properties and Applications. *Renewable Sustainable Energy Rev.* **2015**, *45*, 359−378.
(32) Sermyagina, E.; Saari, J.; Kaikko, J.; Vakkilainen, E. Hydrothermal Carbonization of Coniferous Biomass: Effect of Process Parameters on Mass and Energy Yields. *J. Anal. Appl. Pyrolysis* **2015**, *113*, 551−556.
(33) Parshetti, G. K.; Hoekman, S. K.; Balasubramanian, R. Chemical, Structural and Combustion Characteristics of Carbonaceous Products Obtained by Hydrothermal Carbonization of Palm Empty Fruit Bunches. *Bioresour. Technol.* **2013**, *135*, 683−689.
(34) Di Blasi, C.; Signorelli, G.; Di Russo, C.; Rea, G. Product Distribution from Pyrolysis of Wood and Agricultural Residues. *Ind. Eng. Chem. Res.* **1999**, *38*, 2216−2224.
(35) Hu, B.; Wang, K.; Wu, L.; Yu, S.-H.; Antonietti, M.; Titirici, M.-M. Engineering Carbon Materials from the Hydrothermal Carbonization Process of Biomass. *Adv. Mater.* **2010**, *22*, 813−828.
(36) Titirici, M.-M.; White, R. J.; Falco, C.; Sevilla, M. Black Perspectives for a Green Future: Hydrothermal Carbons for Environment Protection and Energy Storage. *Energy Environ. Sci.* **2012**, *5*, 6796−6822.
(37) Kumar, S.; Loganathan, V. A.; Gupta, R. B.; Barnett, M. O. An Assessment of U(VI) Removal from Groundwater Using Biochar Produced from Hydrothermal Carbonization. *J. Environ. Manage.* **2011**, *92*, 2504−2512.
(38) Parshetti, G. K.; Chowdhury, S.; Balasubramanian, R. Hydrothermal Conversion of Urban Food Waste to Chars for Removal of Textile Dyes from Contaminated Waters. *Bioresour. Technol.* **2014**, *161*, 310−319.
(39) Garg, S.; Jiang, C.; Miller, C. J.; Rose, A. L.; Waite, T. D. Iron Redox Transformations in Continuously Photolyzed Acidic Solutions Containing Natural Organic Matter: Kinetic and Mechanistic Insights. *Environ. Sci. Technol.* **2013**, *47*, 9190−9197.
(40) Voelker, B. M.; Sulzberger, B. Effects of Fulvic Acid on Fe(II) Oxidation by Hydrogen Peroxide. *Environ. Sci. Technol.* **1996**, *30*, 1106−1114.
(41) Kundu, S.; Wang, Y.; Xia, W.; Muhler, M. Thermal Stability and Reducibility of Oxygen-Containing Functional Groups on Multiwalled Carbon Nanotube Surfaces: A Quantitative High-Resolution XPS and TPD/TPR Study. *J. Phys. Chem. C* **2008**, *112*, 16869−16878.
(42) Harvey, A. E.; Smart, J. A.; Amis, E. S. Simultaneous Spectrophotometric Determination of Iron(II) and Total Iron with 1,10-Phenanthroline. *Anal. Chem.* **1955**, *27*, 26−29.
(43) Keenan, C. R.; Sedlak, D. L. Factors Affecting the Yield of Oxidants from the Reaction of Nanoparticulate Zero-Valent Iron and Oxygen. *Environ. Sci. Technol.* **2008**, *42*, 1262−1267.
(44) Trubetskaya, A.; Jensen, P. A.; Jensen, A. D.; Glarborg, P.; Larsen, F. H.; Andersen, M. L. Characterization of Free Radicals by Electron Spin Resonance Spectroscopy in Biochars from Pyrolysis at High Heating Rates and at High Temperatures. *Biomass Bioenergy* **2016**, *94*, 117−129.
(45) Collins, R. L.; Bell, M. D.; Kraus, G. Unpaired Electrons in Carbon Blacks. *J. Appl. Phys.* **1959**, *30*, 56−62.
(46) Wang, L.; Wang, F.; Li, P.; Zhang, L. Ferrous−Tetrapolyphosphate Complex Induced Dioxygen Activation for Toxic Organic Pollutants Degradation. *Sep. Purif. Technol.* **2013**, *120*, 148−155.
(47) Sevilla, M.; Fuertes, A. B. Chemical and Structural Properties of Carbonaceous Products Obtained by Hydrothermal Carbonization of Saccharides. *Chem.—Eur. J.* **2009**, *15*, 4195−4203.
(48) Sun, X.; Li, Y. Colloidal Carbon Spheres and Their Core/Shell Structures with Noble-Metal Nanoparticles. *Angew. Chem., Int. Ed.* **2004**, *43*, 597−601.
(49) Liao, S.; Pan, B.; Li, H.; Zhang, D.; Xing, B. Detecting Free Radicals in Biochars and Determining Their Ability to Inhibit the Germination and Growth of Corn, Wheat and Rice Seedlings. *Environ. Sci. Technol.* **2014**, *48*, 8581−8587.
(50) Montes-Morán, M. A.; Suárez, D.; Menéndez, J. A.; Fuente, E. On the Nature of Basic Sites on Carbon Surfaces: An Overview. *Carbon* **2004**, *42*, 1219−1225.
(51) Chaikin, S. W.; Brown, W. G. Reduction of Aldehydes, Ketones and Acid Chlorides by Sodium Borohydride. *J. Am. Chem. Soc.* **1949**, *71*, 122−125.
(52) Fan, X.; Peng, W.; Li, Y.; Li, X.; Wang, S.; Zhang, G.; Zhang, F. Deoxygenation of Exfoliated Graphite Oxide under Alkaline Conditions: A Green Route to Graphene Preparation. *Adv. Mater.* **2008**, *20*, 4490−4493.
(53) Pavlovič, I.; Knez, Ž.; Škerget, M. Hydrothermal Reactions of Agricultural and Food Processing Wastes in Sub- and Supercritical Water: A Review of Fundamentals, Mechanisms, and State of Research. *J. Agric. Food Chem.* **2013**, *61*, 8003−8025.
(54) Sevilla, M.; Fuertes, A. B. The Production of Carbon Materials by Hydrothermal Carbonization of Cellulose. *Carbon* **2009**, *47*, 2281−2289.

DOI: 10.1021/acsami.7b03310
ACS Appl. Mater. Interfaces 2017, 9, 17115−17124